Mahogany seed – a step forward in deciphering autorotation

Mukul Rao[1], Dhruv C. Hoysall[2] and Jagadeesh Gopalan[2,*]

[1]R.V. College of Engineering, Mysore Road, R.V. Vidyaniketan Post, Bangalore 560 059, India
[2]Department of Aerospace Engineering, Indian Institute of Science, Bangalore 560 012, India

This article presents an experimental approach for evaluating the various flight characteristics of a mahogany seed in its autorotative descent. Analytical formulae proposed by Yasuda and Azuma are used to interpret the results. The findings are used in the development of a sophisticated blade element computational model, primarily to analyse planar autorotating systems. This approximate computational approach is then used to predict the flight performance of mahogany seeds and the results are compared with experimental data. The potential use of the computational model in the design of autorotating systems is then brought to light.

Keywords: Autorotation, computational approach, flight characteristics, mahogany seed.

THE continuous rotation of an object, sustained solely by the influence of aerodynamic forces is termed as autorotation; unless artificially induced (such as in a wind tunnel), this phenomenon is typically observed in falling objects. The rotation might be stable or unstable depending on the physical configuration of the body and atmospheric conditions at the time of descent. Autorotation is observed in nature in varied forms; historically, autorotation of flat plates was the first to spark curiosity in physicists.

Isaac Newton was to describe the complex behaviour of a body freely falling in a fluid medium in *The Principia* (1726). However, it was J. C. Maxwell (1854) who first conducted a systematic study of autorotation[1]; he observed that a flat plate or a card, when dropped would start rotating even when no initial angular velocity was imparted to it. He deduced that the centre of pressure and centre of mass for such plates did not coincide during the fall. Therefore, this produced a torque that triggered the spin.

By the latter half of the 20th century, the autorotation phenomenon in seeds captured the eyes of the scientific community. In particular, the maple seed or the samara became the most widely used seed for experimentation. These seeds have the reputation for descending with extremely low descent velocities and high rates of spin. An auto-rotating seed wing in air is very much like the blade of a windmill. This similarity has led aerodynamicists to employ mathematical models that are used to optimize wind turbine blades, in also modelling the autorotation phenomenon in seeds. Some of these models include the momentum theory and the blade element theory (BET).

In 1973, Norberg[2] conducted the first scientific study of a single-winged samara. He employed the simple momentum theory for analysis and used planar models to mimic the performance of the samara. Two major assumptions were made in his analysis: (1) The samara was a flat wing. (2) The mass of the wing lay on the long axis from the wing root to the wing tip.

Figure 1 shows the force diagram for a samara as presented by Norberg. It is the side view of the seed when it has reached a steady auto-rotational state. At equilibrium, the vertical component of the net lift force F_{AV} balances the weight W of the seed. The resultant components of the centrifugal forces, acting on the right and left side of the centre of gravity (CG) are designated by C_T and C_R respectively. C_T and C_R act through moment arms P_{CT} and P_{CR} respectively, to generate a clockwise moment. This moment is balanced by an anticlockwise moment

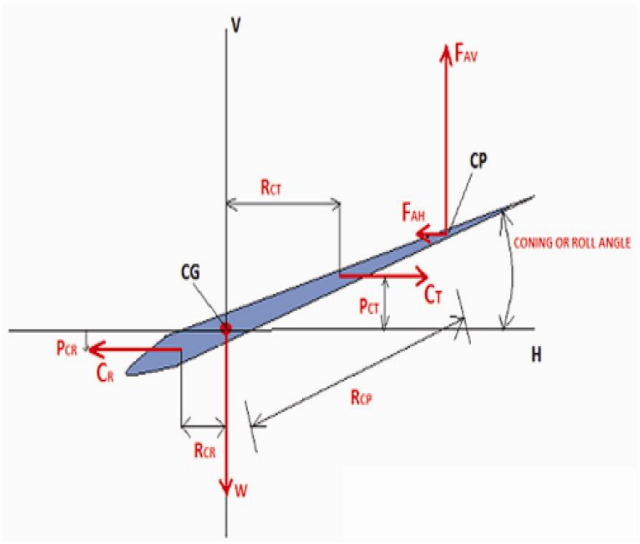

Figure 1. Pictorial representation of the aerodynamic, gravitational and centrifugal forces in a samara[2].

*For correspondence. (e-mail: jaggie@aero.iisc.ernet.in)

created by the action of the net aerodynamic force about the moment arm R_{CP}. Generally, the axis of rotation is slightly displaced away from the CG towards the left, which implies that a net centrifugal force acts towards the right. This force is balanced by the horizontal component of the aerodynamic force F_{AH}. The stable angle created by the seed surface with the horizontal is called the coning angle or roll angle.

In 1989, Azuma and Yasuda[3] conducted a detailed study of the autorotative descent of different samara seeds. They used a camera with a stroboscope flash coupled with a smoked flow observation technique. A simple momentum analysis on the lines of Norberg with the same geometric assumptions helped Azuma and Yasuda to arrive at the optimal expressions for terminal velocity and tip speed.

$$v = \sqrt{\left(\frac{2Mg}{\rho S}\right)}, \tag{1}$$

and

$$V_{\text{tip}} = R\omega = \frac{2^{5/6}}{(\sigma\delta)^{1/3}}\sqrt{\frac{Mg}{\rho S}}. \tag{2}$$

It follows that for a given set of geometric parameters, terminal velocity and angular velocity of a seed cannot be less than that obtained from these expressions.

Seter and Rosen[4] completed a detailed study of autorotational mechanics in 1991. They used a theoretical blade element model with six degrees of freedom analysis for this purpose. In 2007, Andreas Kellas (a graduate student at MIT) made one of the first noteworthy attempts in designing a single-blade autorotating vehicle. This vehicle was to function as a reliable and cost-effective payload drop mechanism that could serve as a viable alternative to the existing ones used by the US army. His work covered several interesting aspects of autorotation such as the coupling of angular velocity components and the effect of control surfaces on the performance of a samara-inspired flight vehicle. He partially succeeded in developing such a vehicle. The flight performance of the vehicle was compared with the results from a numerical model based on the BET[5].

Varshney *et al.*[6] analysed the factors that triggered gyration in maple seeds. The initiation of spin was attributed to the subtle interplay between rigid body dynamics and aerodynamics. This interaction was possible because the asymmetric mass distribution of the seed allowed for the coupling of different angular velocity components.

This summarizes some of the most significant literature available in autorotation. Although extensive work has been done in the area of winged seeds, these efforts only address a small portion of the entire autorotation process. The first purpose of this study is to assess the feasibility of using the well-established momentum theory in evaluating the performance of the seed. A direct outcome of this study would be determination of the operating region of the seed (windmill state, or the turbulent windmill state[5]). This information is vital for employing sophisticated blade element methods to accurately predict the aerodynamic performance of the seeds. This brings us to the second purpose of this study; the presentation of a computational approach based on the modified BET. Although a few papers exist describing the use of BET for evaluating autorotation performance, they describe an oversimplified model that adopts the BET in its original form. The fact that the local wing thrust coefficients can exceed one, leaving the use of the original BET invalid is one of the many factors not taken into account. Further, an extensive comparison of the results from a computational model with experimental data has not been presented before; we do so, by comparing the results with the experimental values for 13 mahogany seed specimens of varying size and geometry. The implications of using this model in such a scenario, its strengths and drawbacks are briefly discussed.

The mahogany seed

The unique geometry of the mahogany seed enables it to autorotate, a fraction of a second after its release. As a consequence, these seeds have low terminal velocities (of the order 0.5–1 m/s), which provide sufficient time for wind gusts to carry them far away from the parent tree, before they touch the ground.

Figure 2 shows the peculiar shape of the seed; it can be seen that its side view mimics the curvature of an airfoil.

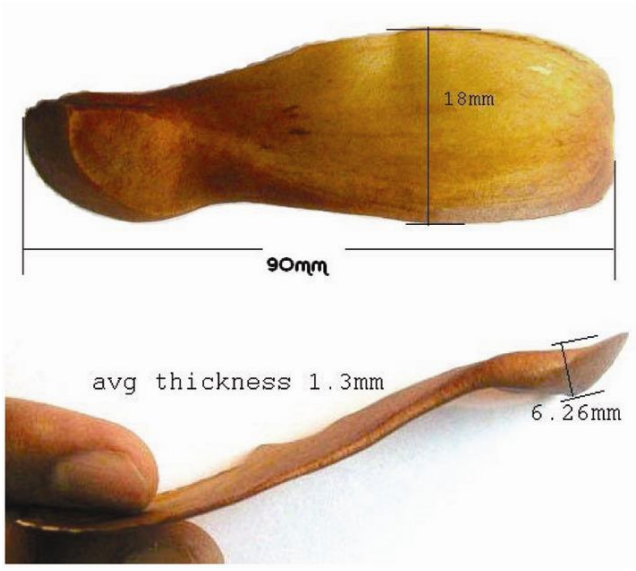

Figure 2. A magnified view of the mahogany seed.

The wing exhibits non-uniform geometry, the leading edge being thicker at the root. The plan view resembles an ellipse. The ribs on the seed 'wing' provide structural strength and also increase the surface roughness. High surface roughness generates beneficial turbulence that improves flight performance[7].

Another striking observation made was that the bulk of the seed mass is located at one end of the seed. According to this mass distribution, about 80–85% of the total mass is located in the 'actual seed' and the remaining mass is distributed in the wing. Figure 3 shows cross-sectional elements obtained by slicing the wing along its span.

We observe from the figure that the pieces to the right have distinct airfoil shapes. The pieces to the left are much thicker and harbour majority of the total seed mass. The length of this particular seed is 80 mm and the calculated centre of mass is 17 mm from the origin, i.e. within the first four slices (Table 1; see supplementary material, online).

Experiment set-up

The seeds to be tested were split into three groups based on their mass – group 1: 0.45 to 0.5 g; group 2: 0.35 to 0.45 g and group 3: 0.3 to 0.35 g. Only fully developed seeds were considered. The dimensions of the seeds were measured using a digital vernier caliper (least count = 0.1 mm) and the mass was measured with an electronic balance (least count = 0.001 g).

Figure 4 shows a schematic diagram of the experimental set-up. It consists of a high-speed camera capable of taking pictures at one million frames per second. The camera was set to take pictures at 200 frames per second and at an exposure time of 400 ms. The picture frames were stored in a digital format (*.cci). The camera photographed a region approximately 50–82 cm from the point where the seed was dropped. Since the exposure time was small, an external light source of 350 W (extremely bright) was used for lighting. Attempts were made to photograph two envisaged phases of the seed fall and flight. The objective was to find out how the seed begins to autorotate from a free-fall mode and to understand how the seed behaves when it has reached a steady state.

Figure 3. Cross-sectional elements of the wing.

A total of 13 seeds were dropped from a fixed height/datum and at a fixed inclination with the vertical (exactly vertical with zero angle of attack and seed facing downward). As these seeds are curved, it is difficult to determine what 0 angle of attack means; all seeds were dropped such that the lower part of the seeds was in line with the vertical. A soft landing spot was made for the seeds such that they would not break when they hit the ground. The seeds were dropped in still air by carrying out these trials in a closed room. This method was adopted to ensure that their flight characteristics were not affected by draughts of wind. The results are tabulated in Tables 2 and 3 in supplementary material (see online).

Comparative study

A comparative study was done between the experimental data and the theoretical values derived from the expressions proposed by Azuma and Yasuda. The results from this study are depicted graphically.

Figure 5 shows the variation of terminal velocity of the 13 mahogany seeds with disc loading. The blue points indicate the performance of the seeds, whereas the red line represents the variation of optimum terminal velocity with disc loading as proposed by Azuma and Yasuda's theory. According to this theory, the minimum terminal velocity is given by

$$V = \sqrt{\frac{2Mg}{\rho S}}, \tag{3}$$

or

$$V = \sqrt{\frac{2 \times \text{discloading}}{\rho}}, \tag{4}$$

where discloading = Mg/s.

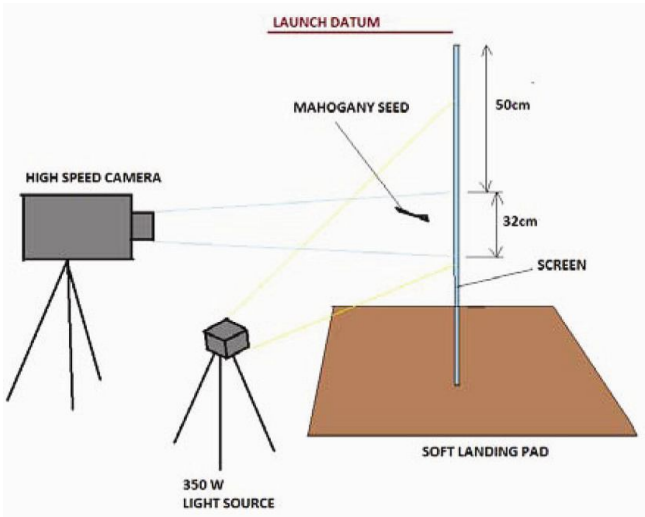

Figure 4. Experimental set-up.

We observe that four seeds have a descent velocity smaller than that proposed by Azuma and Yasuda's and hence a positive error. The reason for this deviation becomes evident when one considers the limitations of the momentum theory, which serves as the basis for Azuma's theoretical expressions. A key assumption made in this theory is that the streamlines are definite and smooth as they cross the rotor blade[7].

Figure 6 shows the two possible descent states of the mahogany seed according to the classic rotor craft and windmill theory. In the windmill state, the descent velocity V is large enough to overpower the induced velocity υ and the streamlines flow smoothly through the disc traced by the seed wing. However, in the turbulent windmill state, the streamlines are not smooth and there are regions where there the flow is chaotic with areas of recirculation. This case occurs when $V < \upsilon/2$.

Considering the windmill state, the thrust equation according to the momentum theory[3] is given by

$$T = 2\rho S(V - \upsilon)\upsilon, \tag{5}$$

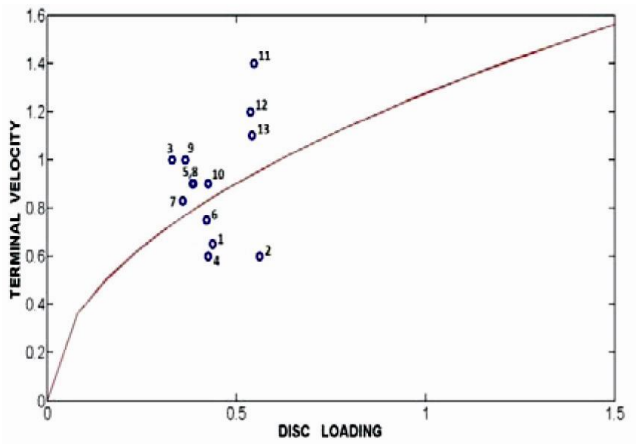

Figure 5. Experimental and theoretical terminal velocity.

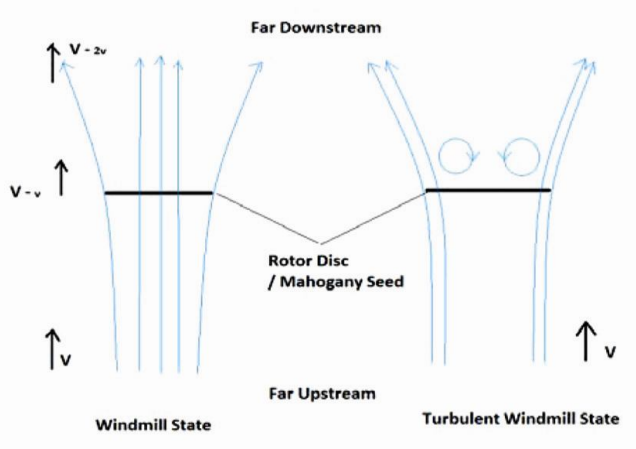

Figure 6. The two possible descent configurations.

where V is the free stream velocity, which in this case is the vertical descent velocity of the seed. At optimum velocity of descent, all the kinetic energy is extracted from the flow, in which case the velocity far downstream of the seed reduces to zero.

$$V - 2\upsilon = 0 \text{ or } \upsilon = V/2. \tag{6}$$

Indeed, if this is substituted in eq. (6), we arrive at Azuma and Yasuda's expression for optimum velocity, i.e. eq. (3).

For a more general case, let the induced velocity be expressed in terms of the free stream velocity by the relation

$$\upsilon = aV, \tag{7}$$

where a is the axial induction factor. Substituting this in the thrust equation and modifying, we get

$$C_T = 4a(1 - a), \tag{8}$$

where $C_T = T/((1/2)\rho SV^2)$ is called the thrust coefficient.

Equation (9) is valid only when $0 \le a \le 0.5$ or equivalently $0 \le \vartheta \le V/2$. Azuma and Yasuda's operating point is given by $a = 0.5$ and $C_T = 1$.

What happens to the thrust coefficient when a crosses 0.5, i.e. when the seed enters the turbulent windmill state?

Figure 7 shows the variation of C_T with a. Beyond $a = 0.5$, the momentum equation under predicts the thrust coefficient. The correct C_T values are obtained experimentally and proven to be higher (see the dotted points on the graph). Clearly, the momentum curve (shown in pink) travels beneath these points. In fact, the answer becomes evident when the thrust coefficient is calculated for each seed (Figure 8).

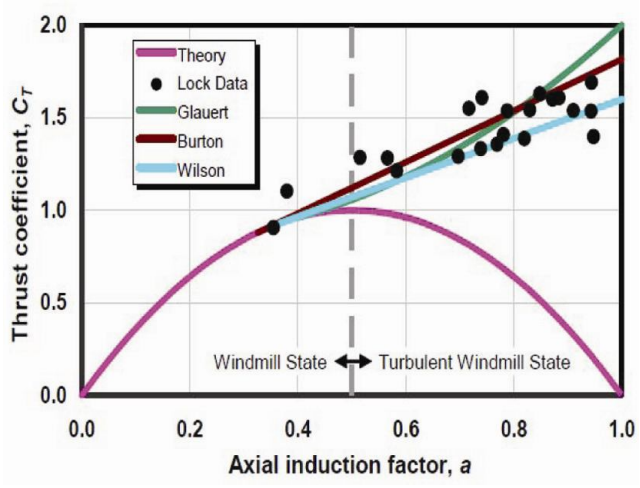

Figure 7. Theoretical and experimental thrust coefficient in the two descent states (courtesy: Buhl[8], National Renewable Energy Laboratory).

All seeds (1, 2, 4 and 6) that showed a positive error have their experimental thrust coefficients greater than one. Consequently, Azuma and Yasuda's theory failed to predict the correct descent values for these seeds because they were operating far beyond the theory's limitation.

Figure 9 shows the plot of tip speed versus disc loading. The solid line represents the tip speed according to Azuma and Yasuda's theory and is given by

$$V_{\text{tip}} = R\omega = \frac{2^{5/6}}{(\sigma\delta)^{1/3}}\sqrt{\frac{Mg}{\rho S}}, \tag{9}$$

or

$$V_{\text{tip}} = R\omega = \frac{2^{5/6}}{(\sigma\delta)^{1/3}}\sqrt{\frac{\text{DiscLoading}}{\rho}}. \tag{10}$$

The curve is plotted assuming $\sigma\delta$ to be equal to 0.05.

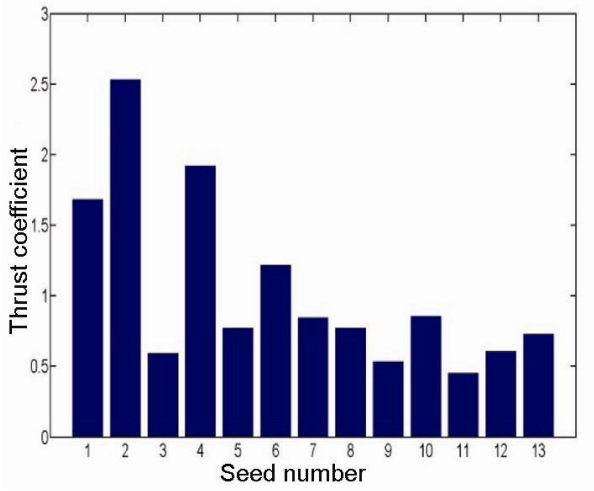

Figure 8. Net thrust coefficient.

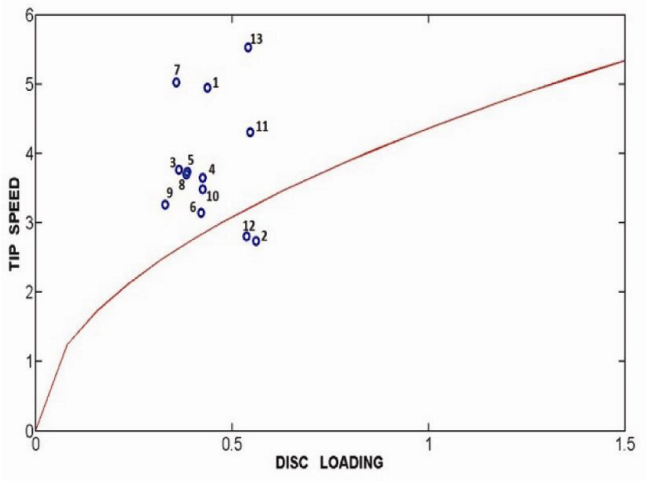

Figure 9. Experimental and theoretical tip speed.

Most of the seeds had tip speeds greater than that predicted by this equation. A comparative study might not be meaningful in this case because each seed has a different solidity σ and aerofoil properties (and hence different δ). Figure 10 shows a bar chart depicting the tip-speed error for each seed. The solidity of each seed was calculated using the formula

$$\sigma = \frac{B_{\max}}{\pi R}. \tag{11}$$

The δ value is assumed to be equal to 0.5.

Conclusion from comparative study and motivation for a computational model

The comparative study revealed that the mahogany seeds operate in both the windmill state and turbulent windmill state. Therefore, the classic BET is not always applicable and a more realistic blade element formulation is required that can model aerodynamic forces even in the turbulent windmill state. One such scheme is the WT_PERF algorithm, a description of which can be found in Buhl[8]. It is evident that simplistic models like that of Azuma require the angular velocity and disc diameter before some analysis can be performed. In this work, these parameters were obtained with a high-speed camera. However, this method of analysis is not elegant. A more comprehensive approach would be to solve for all these parameters simultaneously using a numerical method. Essentially, we solve a giant initial value problem. A brief description of the model is given below. A detailed explanation of the work can be found in Rao[9].

The computational model

Two frames of reference are used in the numerical analysis. The first frame is the inertial frame/global frame *XYZ*

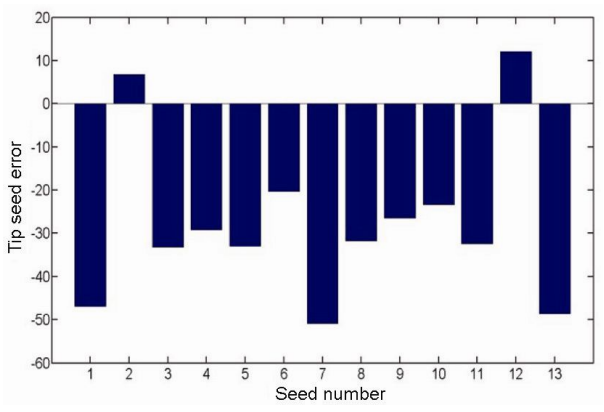

Figure 10. Deviation (in %) between theoretical and experimental values.

attached to a stationary observer on Earth. The second frame *xyz*, referred to as the body frame, is attached to the autorotating object, which in this case, is a two-dimensional wing that is an approximate representation of the mahagony seed (Figure 11).

The motion of the seed is determined by the solution of three well-known vector differential equations that represent the dynamics of a rigid body in the body frame system of coordinates.

Linear momentum equation: $\vec{f} = \overrightarrow{vcm} + \vec{w} \times \overrightarrow{vcm}$, (12)

Angular momentum equation: $\overrightarrow{Tb} = I\vec{w} + \vec{w} \times I\vec{w}$, (13)

Quaternion angular velocity relation: $\vec{Q} = \frac{1}{2}[0\ \vec{W}]\phi\vec{Q}$. (14)

Equation (14) represents the change in orientation of the system and is required for mapping vectors between the two frames of reference and ϕ is the quaternion multiplication factor. To integrate eqs (12–14), a first-order approximation for the force and torque vector is used, i.e. they are kept constant over a small time-interval. The modified equation can then be integrated using a higher-order scheme to yield new values for $\overrightarrow{vcm}$, $\vec{w}$ and $\vec{Q}$. The force and torque vectors are then updated using these values and the next time-advancement step is performed. To update the force and torque vectors, we make use of the panelling approach in conjunction with the WT_PERF algorithm. The initial conditions used in the simulations are $\overrightarrow{v_{cm}} = 0$, $\vec{w} = 0$ and $\vec{Q} = [1000]$.

The MATLAB ode15s solver is used to solve the system of differential equations. The relative and absolute error tolerances were kept at their default values of 10^{-3} and 10^{-6} respectively. ode15s is a variable-order solver based on the numerical differentiation formulas (NDFs). It is particularly useful in solving a stiff system of differential equations.

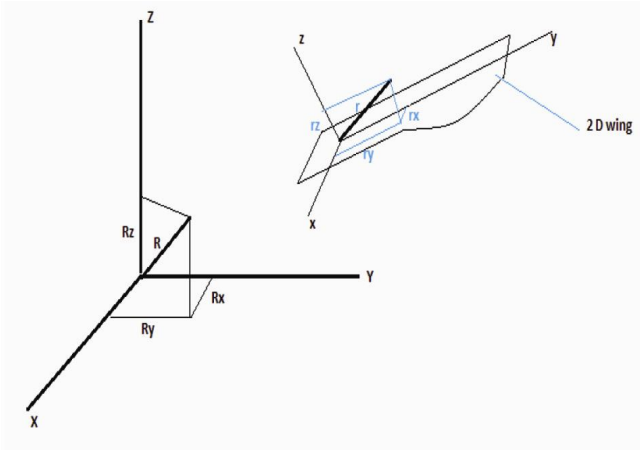

Figure 11. Vector *R* in the global and local coordinate system.

Local coordinate system positioning

The 2D wing system consists of a point mass *m* that carries 80–90% of the total seed mass *M*. The remaining mass (20–10%) is distributed uniformly along the wing surface. The wing has a NACA 0012 cross-section and for the purposes of our calculations, the thickness was neglected in the inertia calculations. The reason for choosing a NACA 0012 airfoil was that there was reliable lift, drag and quarter chord moment coefficient data available from the National Renewable Energy Laboratory (NREL) at a low Reynolds Number for the full range of angle of attack. A flat plat airfoil would have been ideal but a reliable source of airfoil performance could not be found for the full range of angle of attack. The location of point mass can be varied to position the centre of mass (COM) at any desired point (x_{cm}, y_{cm}) with respect to the axes x_1y_1. The point load was positioned based on the co-ordinates with reference to the axes x_1y_1. Once the point load was fixed, the CG was calculated and the local coordinate system *xyz* was positioned about the CG. The local coordinate system has its origin at the COM and is orientated as shown in Figure 12. The axes *z* and z_1 point out of the plane of the paper, towards the observer. The wing is divided into 101 panels along its span.

The inertia matrix I_0 is first calculated about axes $x_1y_1z_1$ and when the COM position is set, the inertia matrix *I* (used in eq. (13)) is determined about the local coordinate system *xyz* using the parallel axis theorem.

Calculating force and torque

The aerodynamic forces considered in the panelling approach are only those resolved in the *xz* plane. The spanwise components (along *y*) are neglected.

The net force and torque are computed by taking into account the aerodynamic forces and torques produced by all panels and summing them up (Figure 13). The gravitational force contribution is then added to this sum to form the net force. These calculations are done in the body frame of reference. To compute the aerodynamic forces, we need the impinging velocity vector at the leading edge of each panel. The impinging velocity vector is comprised of two components – one due to rigid body rotation and the other due to the induced velocity (Figure 14). The rigid body component can be calculated using:

$$v_r = v_{cm} + \omega \times r. \quad (15)$$

The induced velocity component is calculated using the PERF algorithm. Once the velocity vector is known, the real angle of attack (Figure 15) can be calculated and with the NACA 0012 properties, the lift, drag and quarter

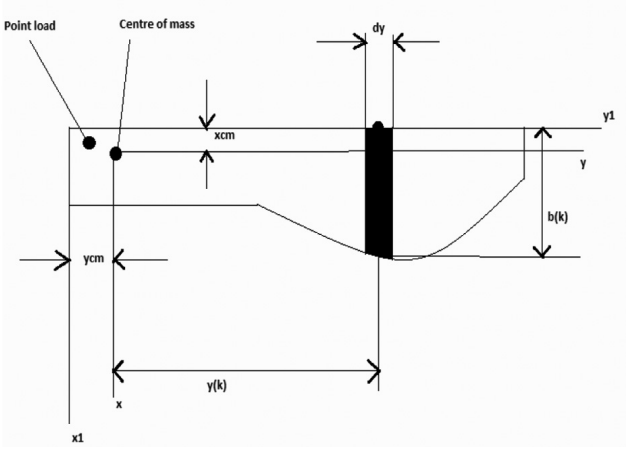

Figure 12. Various parameters as viewed in the local coordinate system.

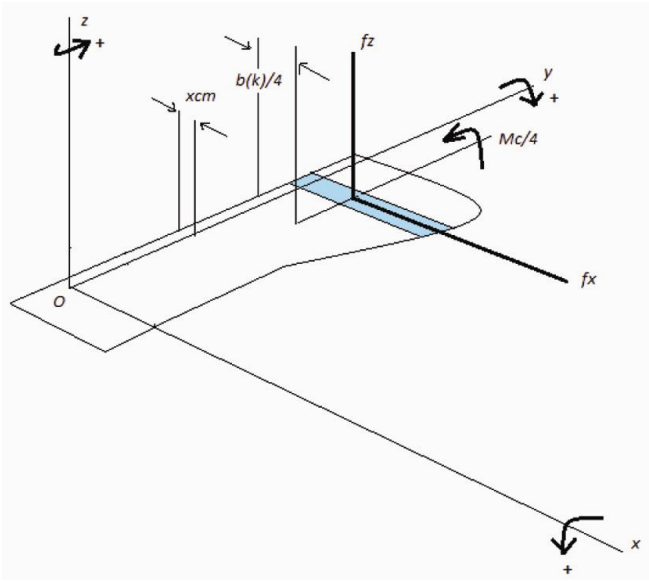

Figure 13. Forces acting on a blade element.

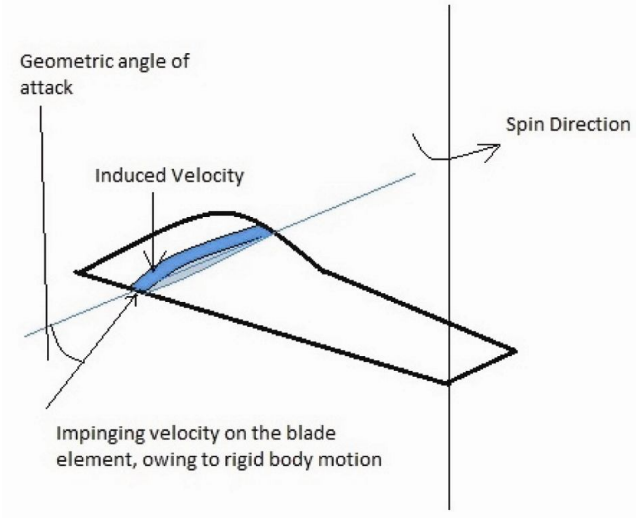

Figure 14. Velocity vectors impinging on a blade element.

chord moment coefficients are known at each panel; the aerodynamic forces and moments can now be calculated.

The net aerodynamic force in the body frame is thus given by

$$\begin{bmatrix} f_x \\ f_y \\ f_z \end{bmatrix} = \begin{bmatrix} \sum_1^{101} (D'(k)\cos\alpha_r(k) - L'(k)\sin\alpha_r(k)) \\ \sum_1^{101} (L'(k)\cos\alpha_r(k) + D'(k)\sin\alpha_r(k)) \end{bmatrix}, \quad (16)$$

where the terms within brackets indicate resolved components of lift and drag along the x and z directions.

From Figure 14, it can be easily seen that the aerodynamic moments are given by

$$\begin{bmatrix} T_x \\ T_y \\ T_z \end{bmatrix} = \begin{bmatrix} \sum_1^{101} f_z(k) y(k) \\ -\sum_1^{101} f_z(k)\left(\frac{b(k)}{4} - x_{cm}\right) + \sum_1^{101} M_{c/4}(k) \\ -\sum_1^{101} f_x(k) y(k) \end{bmatrix}, \quad (17)$$

where

$$M_{c/4}(k) = \frac{1}{2}[C_{m_{c/4}}(\alpha_r(k))]\rho(v_{chord}(k))^2 b(k)^2 dy. \quad (18)$$

Results from the numerical method

The results are shown in Table 4 in supplementary material (see online). The performance plots obtained for seed1 are shown in Figures 16–20. From Figure 16 one can see the COM (green curve) trace an initial vertical trajectory under the influence of gravity for a short distance

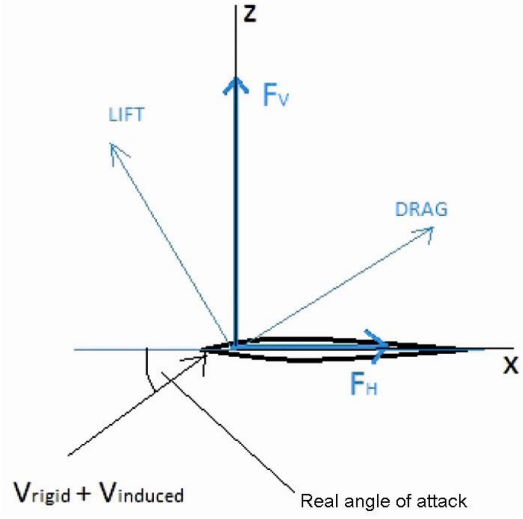

Figure 15. Net velocity and real angle of attack.

(<0.5 m), and later trace a helix once the centrifugal forces are set up. We need to keep in mind that the three coordinate axes have different scaling. A better visualization of the solution trajectory can be observed from Figure 17.

Figure 18 shows the time history of the global Z component of velocity. Initially it is linear, predominantly under the influence of gravity. Once the spin rate develops, the magnitude drops and reaches a stable value. This is the terminal velocity of the seed. In Figure 19, the negative spin rate indicates a clockwise spin direction.

The corresponding global Z-component of acceleration (Figure 20) starts at –9.81 m/s^2 and increases to positive values. When a mahogany seed falls, it initially plummets under the influence of gravity. Once the aerodynamic forces develop, its descent rate drops and stabilizes. This 'recovery' phase has positive acceleration associated with it in the global Z direction. Once equilibrium is attained, the acceleration drops to zero.

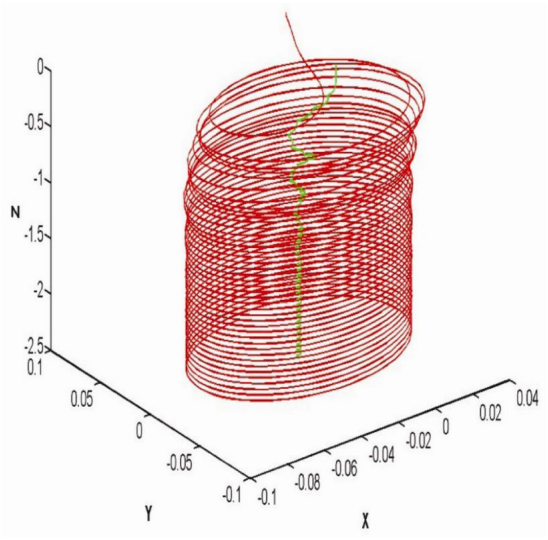

Figure 16. Trajectory of the centre of mass and wing tip. All dimensions in metres. Direction of spin is clockwise.

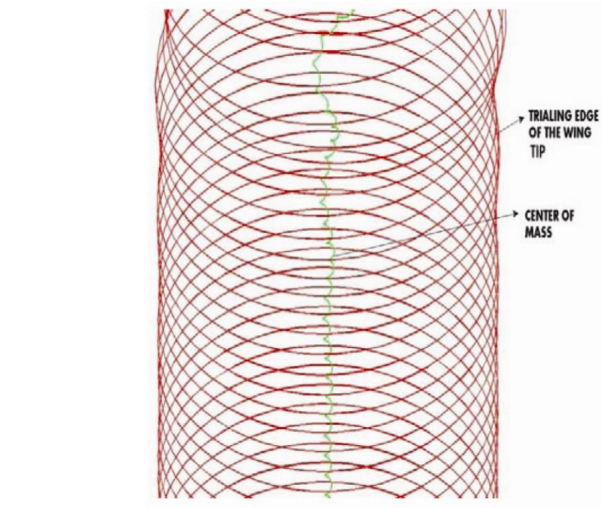

Figure 17. Trajectory of the centre of mass and wing tip trailing edge (magnified view).

Drawbacks and application

Although the results are highly encouraging, one must still recognize the drawbacks of the approximate approach:

(i) The real flow is three-dimensional over the blade element and the spanwise forces are neglected in our model. Also, the velocity over the blade is not a constant due to variation in spin vector contribution.

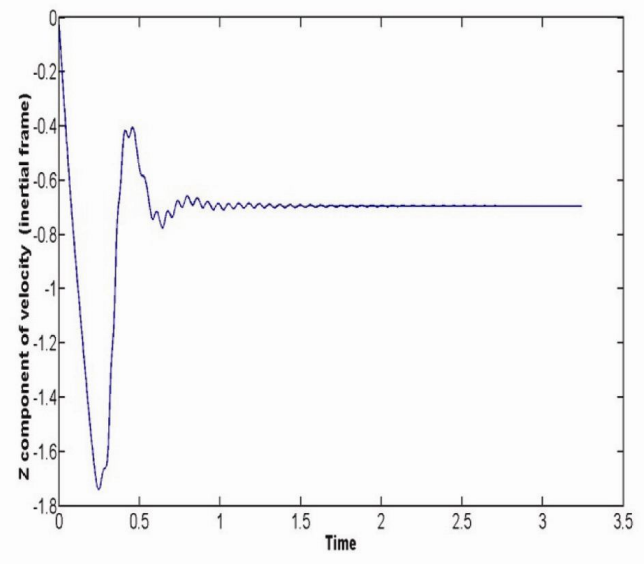

Figure 18. Terminal velocity.

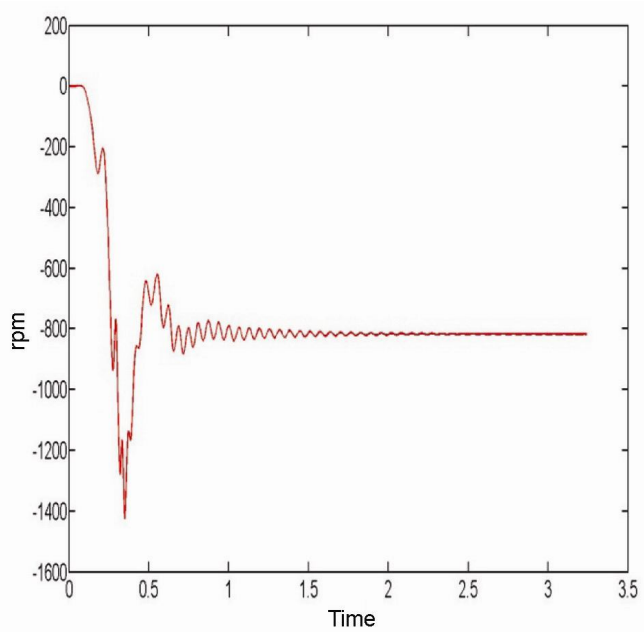

Figure 19. Spin rate at equilibrium.

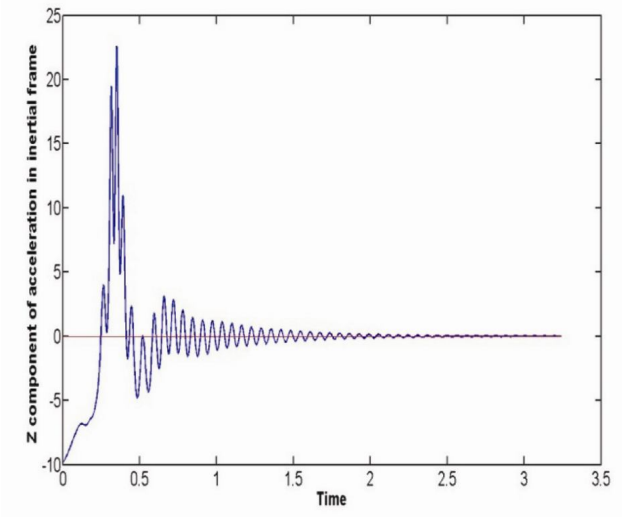

Figure 20. Zero acceleration in the *Z* direction at equilibrium.

(ii) We have approximated the mahogany seed with a simplistic planar model. However, the grand scheme can be extended to account for 3D geometry provided the aerodynamic model is replaced with a superior one.

When one attempts to design an autorotating system, the mass distribution for a given wing planform and cross-section, cannot be arbitrary. There is a fixed region within which bulk of the mass must be distributed. This is referred to as the autorotation boundary[10]. The computational model helps estimate this region. In the case of the planar wing loaded with a point mass, violent oscillations were observed in the solutions when the point load was placed in unfavourable regions, indicating that for the given configuration an equilibrium point could not be attained. Thus this program can be used as a rough estimate to determine autorotation boundaries.

Conclusion and scope for further work

An experimental study was conducted and the performance of mahogany seeds was determined. A comparison with the theoretical results showed that the simplified momentum theory served as a poor basis to evaluate the flight characteristics of these seeds. The calculation of the thrust coefficients revealed that the seeds operated in both the windmill and the turbulent windmill state. Therefore, a more sophisticated wind turbine performance evaluation method such as the modified blade element theory was employed to gauge the performance of the mahogany seed with reasonable success. The crux of the approach presented can be extended to incorporate a Computational Fluid Dynamics model (which replaces the modified BET for evaluating the aerodynamic forces and torques). This would require the use of a grid that continuously adapts in each iteration (time interval) and that takes into account the new seed orientation and the free stream condition at each grid point. The use of such a rigorous approach would then reveal the true trajectory of the seed during its fall. Development of the three-dimensional boundary layer over the seed surface can also be visualized in the process.

1. Maxwell, J. C., On a particular case of the descent of a heavy body in a resisting medium. *Cambridge. Dublin Math. J.*, 1894, **9**, 145–148.
2. Norberg, R. A., Autorotation, self stability and structure of single-winged fruits and seeds (Samaras) with comparative remarks on animal flight. *Biol. Rev*., 1973, **48**, 561–596.
3. Azuma, A. and Yasuda, K., Flight performance of rotary seeds. *J. Theor. Biol.*, 1989, **138**, 23–53.
4. Seter, D. and Rosen, A., Study of the vertical autorotation of a single winged samara. *Biol. Rev*., 1992, **67**, 175–197.
5. Gessow, A. and Meyers Jr, G. C., *Aerodynamics of the Helicopter*, Frederich Ungar Publishing Co.
6. Varshney, K., Chang, S. and Jane Wang, Z., The kinematics of falling Maple seeds and the initial transition to a helical motion. *IOP Science*, 25, C1.
7. Lorenz, R. D., *Spinning Flight: Dynamics of Frisbees, Boomerangs, Samaras, and Skipping Stones*, Springer, pp. 271–289.
8. Buhl, M. L., A new empirical relation between thrust coefficient and induction factor for the turbulent windmill state. Technical Report, NREL/TP 500-36834.
9. Rao, Mukul, The aerodynamics of the Sweitenia mahogany seed. Project Report, Department of Aerospace Engineering, IISC, Bangalore, 2012.
10. Azuma, A. and Yasuda, K., The autorotation boundary in the flight of samaras. *J. Theor. Biol*., 1997, **185**, 313–320.

Received 27 June 2013; accepted 19 December 2013